

Sensitivity of the FCC-ee to the decay of a dark photon into a $\mu^+\mu^-$ pair

G. Polesello^{1*}

¹INFN Sezione di Pavia, Via Bassi 6, 27100 Pavia, Italy.

Corresponding author(s). E-mail(s): giacomo.polesello@cern.ch;

Abstract

The production of a dark photon A' at the proposed CERN FCC-ee collider is investigated. The study addresses the associated production $e^+e^- \rightarrow \gamma A'$ followed by the decay $A' \rightarrow \mu^+\mu^-$. The 95% CL sensitivity on the mixing between the photon and the dark photon is evaluated in the $m_{A'}$ mass range 0.4-360 GeV, based on a parametrised simulation of the IDEA detector. The study is performed both for prompt and long-lived decays of the A' .

1 Introduction

The next generation of high-energy particle colliders is under active discussion in the particle physics community. A very attractive option that is being discussed is e^+e^- circular colliders, such as the CERN FCC-ee [1]. These machines will provide access to a broad range of physics studies, from precision measurements of the Higgs boson and of Standard Model (SM) parameters, to direct searches for physics beyond the Standard Model (BSM).

An interesting group of BSM models are the dark sectors [2, 3], which are well-motivated candidates to explain the observed abundance of dark matter. In dark sector models the SM interacts with dark matter through a weakly coupled SM neutral mediator. Different scenarios have been proposed, corresponding to different types of mediators. The Higgs, vector, and neutrino portals, where the mediator is, respectively, a scalar, a vector, and a fermion field have been the subject of intense phenomenological investigation.

The present study aims at evaluating the sensitivity to the production of vector mediators at the FCC-ee. All of the FCC-ee runs are considered, namely the Z -pole, WW , ZH and $t\bar{t}$, at centre-of-mass energies respectively of $\sqrt{s} = 91.2, 160,$

240 and 365 GeV and with target integrated luminosities respectively of $L_{int} = 205, 19.2, 10.8, 2.7 \text{ ab}^{-1}$. [4]

We focus on a specific implementation of the vector portal, the so-called dark photon or hypercharge portal, as defined in [5]. The dark photon mass region ranging from 0.4 to 360 GeV is investigated for this model, based on the study of the process $e^+e^- \rightarrow \gamma A'$ followed by the decay $A' \rightarrow \mu^+\mu^-$. The decay into muons is expected to provide better sensitivity than the decays into electrons, taus or hadrons, because of lower backgrounds and more precise experimental reconstruction of the final state, yielding better separation power of signal from background. A significant additional sensitivity is however expected from the consideration of all of the A' decay modes, and detailed analyses in this direction are a possible future development of the present study.

The phenomenology of the model and the status of the experimental searches are reviewed in detail in [6] and [7]. Phenomenological studies addressing the $A' \rightarrow \mu^+\mu^-$ signature at future e^+e^- colliders are documented in [8] and [9].

We extend and complete the previous work by assessing the experimental reach of the FCC-ee based on a detailed parametrised simulation of the proposed IDEA detector [10] and on the consideration of the leading backgrounds for all the FCC-ee runs. This approach provides a realistic estimate of the discovery potential and it highlights the dependence of the result from key elements of the detector performance. In particular, the crucial resolution on the two-muon invariant mass is evaluated on the basis of the simulation of the muon track measurement in the tracker of the IDEA detector. The complete kinematics of the events is used in order to separate the signal from the backgrounds, rather than only exploiting the mass constraints, yielding a significant improvement on the results of [9].

In addition, exploiting the excellent vertexing capabilities of the IDEA detector, a detailed experimental analysis targeting long-lived decays of the dark photon is developed. This analysis gives access to an area of the parameter space of the benchmark model which is outside of the reach of projected collider and beam dump experiments, and was not considered in previous publications.

The paper is organised as follows: the effective dark photon model is first introduced and briefly discussed. In the following sections the Monte Carlo event generation is discussed, followed by a description of the adopted approach to detector simulation. On this basis, analyses targeting prompt and long-lived signatures are developed in the following sections. Finally, the additional coverage of FCC-ee with respect to the projections for the main experiments expected to take data in the coming years is assessed for the studied benchmark model.

2 The model and its parameters

The benchmark model addressed in the present study is defined in [5]. It implements kinetic mixing between a broken dark Abelian gauge symmetry, $U(1)_D$, and the SM hypercharge, $U(1)_Y$. The relevant gauge terms in the Lagrangian are

$$\mathcal{L} \subset -\frac{1}{4} \hat{B}_{\mu\nu} \hat{B}^{\mu\nu} - \frac{1}{4} \hat{Z}_{D\mu\nu} \hat{Z}_D^{\mu\nu} + \frac{1}{2} \frac{\epsilon}{\cos\theta} \hat{Z}_{D\mu\nu} \hat{B}^{\mu\nu} + \frac{1}{2} m_{D,0}^2 \hat{Z}_D^\mu \hat{Z}_{D\mu}. \quad (2.1)$$

Here the hatted fields indicate the original fields with non-canonical kinetic terms, before any field redefinitions. The $U(1)_Y$ and $U(1)_D$ field strengths are respectively $\hat{B}_{\mu\nu} = \partial_\mu \hat{B}_\nu - \partial_\nu \hat{B}_\mu$ and $\hat{Z}_{D\mu\nu} = \partial_\mu \hat{Z}_{D\nu} - \partial_\nu \hat{Z}_{D\mu}$, θ is the Weinberg mixing angle, and ϵ is the kinetic mixing parameter. After electroweak symmetry breaking three neutral gauge bosons are present in the model: the photon, the Z , and a dark photon, which will be called A' in the following.

The leading order couplings of the dark photon to fermions are calculated in [5], they are proportional to ϵ and depend on the ratio of $m_{A'}$ and m_Z . For $\epsilon \ll 1$ and $m_{A'} \ll m_Z$ the couplings are photon-like, and they evolve towards Z -like as $m_{A'}$ approaches m_Z . The leading order calculation does not provide an accurate prediction of the dark photon width and its branching fraction into muons for $m_{A'} < 10$ GeV. It is in fact necessary to account for the hadronic resonances into which the dark photon dominantly decays if its mass is close to the resonance mass. A detailed calculation is provided in [5], together with a computer-readable table of widths and branching fractions for $m_{A'}$ in the range 0.36-88 GeV, which will be used throughout this paper. A comparison of $BR(A' \rightarrow \mu^+ \mu^-)$ as calculated in [5] with the leading order one, as implemented by the same group in the MG5aMC@NLO generator, is shown in Figure 1. The latter gives a constant value of 0.25 for $m_{A'} < 3$ GeV, whereas the full calculation exhibits a complex structure, with large dips for masses corresponding to the masses of the ω (782.6 MeV) and ϕ (1020 MeV) resonances.

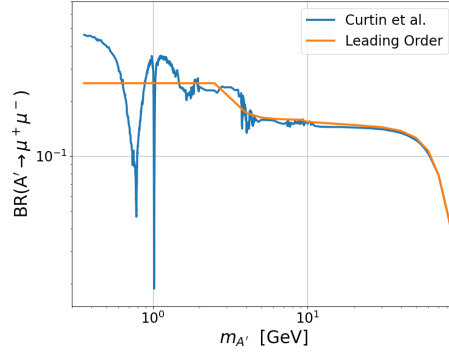


Fig. 1 Value of $BR \rightarrow \mu^+ \mu^-$ as calculated in [5] (blue) and leading order calculation as implemented in MG5aMC@NLO (orange) as a function of $m_{A'}$.

The resulting values of the A' cross-section for $\sqrt{s} = 91.2$ GeV and total width $\Gamma_{A'}$ are proportional to ϵ^2 , and are shown in Figure 2 for $\epsilon = 1$.

From the total width, the decay length of the A' $L_{A'}$ can be calculated as:

$$L_{A'} = \frac{\sqrt{\gamma^2 - 1}}{\Gamma_{A'}},$$

where γ is the relativistic boost factor of the A' . The value of $L_{A'}$ in the $m_{A'} - \epsilon$ plane calculated for the process $e^+ e^- \rightarrow \gamma A'$ at $\sqrt{s} = 91.2$ GeV is shown in Figure 3.

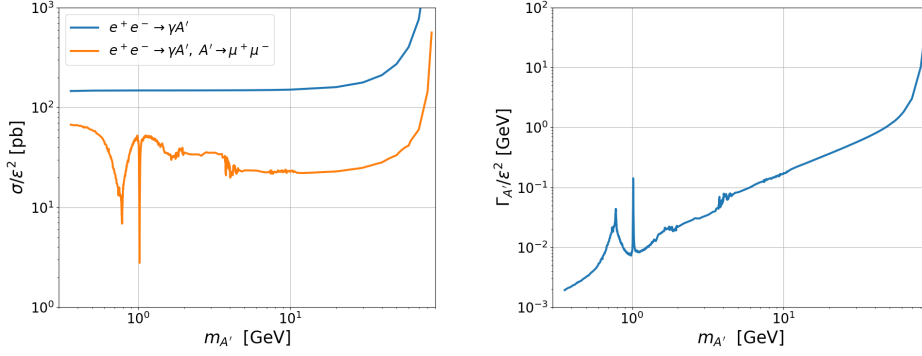


Fig. 2 Left: Cross-section for A' production in pb divided by ϵ^2 as a function of $m_{A'}$. Right: Width in GeV of the A' divided by ϵ^2 as a function of $m_{A'}$.

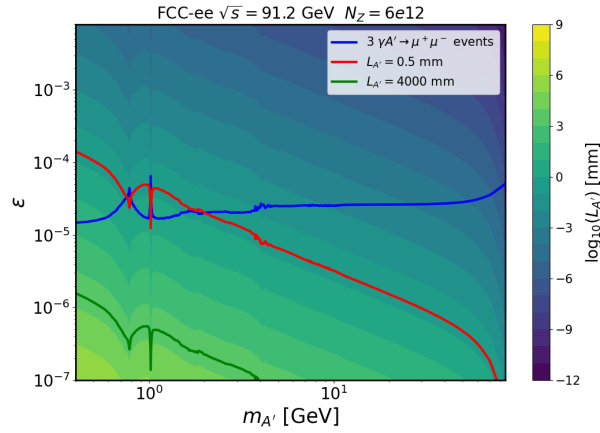


Fig. 3 $L_{A'}$ in the $m_{A'}$ – ϵ plane calculated for the process $e^+e^- \rightarrow \gamma A'$ at $\sqrt{s} = 91.2$ GeV. The red and the green line bound the area in the parameter space where a long-lived A' search can be performed, and the blue line shows the parameters corresponding to the production of 3 events for the expected FCC-ee statistics of 6×10^{12} Z bosons.

From this plot the theoretical parameter space accessible to FCC-ee searches can be evaluated. The blue line shows the values of $m_{A'}$ and ϵ yielding 3 events for the Z -pole run. Over the full mass range up to the Z mass, in absence of background, the minimum reachable value of ϵ is a few 10^{-5} .

The approximate region over which the A' decays inside the detector with an observable flight path is comprised between the red line, corresponding to $L_{A'} = 0.5$ mm, and the green line, corresponding to $L_{A'} = 4$ m. A useful number of long-lived events may thus be observed inside the triangle bounded from above by the red line, and from below by the blue line, which extends up to $m_{A'}$ of a few GeV. This region has discontinuities for masses where the A' mainly decays into hadronic

resonances, due to the combined effect of lower production rate for the muon channel and of shorter lifetime.

3 Signal and background generation

The signal samples were generated with MG5aMC@NLO [11], based on the model files made available in [12]. The model includes both a dark photon and a dark Higgs, and has four parameters, $m_{A'}$ and ϵ for the dark photon sector, the mass of the dark Higgs H_s , and its coupling κ . The latter two parameters are set respectively at 1 TeV and 10^{-9} , decoupling the dark Higgs sector from the analysis.

The generated process was:

$$e^+e^- \rightarrow \gamma A', A' \rightarrow \mu^+\mu^-$$

Scans were performed over $m_{A'}$ between 0.5 and 360 GeV, generating for each of the centre-of-mass energies of 91.2, 160, 240 and 365 GeV a grid of the kinematically accessible mass values. The mixing of the A' with the photon ϵ was set to 10^{-4} , near the minimum value of ϵ explored in the analysis. A total of 100k events per point were generated for these samples.

For the long-lived analysis, samples of 100k events for masses between 0.4 and 1.6 GeV with a granularity of 0.1 GeV were generated, for a grid of values of ϵ varying between $10^{-3.5}$ and 10^{-5} at $\sqrt{s} = 91.2$ GeV.

The parton-level events were hadronised with PYTHIA8 [13] and then fed into the DELPHES [14] fast simulation of the IDEA Detector [10], based on the official datacards used for the "Winter2023" production of the FCC-PED study [15].

For the prompt analysis the irreducible background from the process

$$e^+e^- \rightarrow \gamma \mu^+\mu^-$$

was produced at leading order (LO) with MG5aMC@NLO. The generation-level requirements were that photons and leptons be produced within a pseudorapidity η of ± 2.6 , corresponding to a polar angle of approximately 10° from the beam, and that the photon (muon) energy be in excess of 5 (0.5) GeV, respectively. Samples of 10M events were produced for each of the considered centre of mass energies, 91.2, 160, 240 and 365 GeV. For the Z-pole run an additional 10M background sample with the requirement $m_{\mu^+\mu^-} < 15$ GeV was generated to ensure enough Monte Carlo statistics in the $m_{\mu^+\mu^-}$ mass bins below 20 GeV.

For the long-lived analysis, a sample of 50M $e^+e^- \rightarrow \gamma \mu^+\mu^-$ events were generated at 91.2 GeV, with the additional requirement that $m_{\mu^+\mu^-} < 4$ GeV, and $44.5 < E_\gamma < 46.5$ GeV. The cross-section for this sample is 0.63 pb, and the generated statistics corresponds to an integrated luminosity of 80 ab^{-1} .

Two samples of 10M events for the processes $e^+e^- \rightarrow \gamma \tau^+\tau^-$ and $e^+e^- \rightarrow \gamma b\bar{b}$ with the same requirements on the photon energy were also generated to check the reducible backgrounds to the long-lived analysis. For both samples the generated statistics corresponds to several times the expected statistics for the Z-pole run.

All the background samples were then processed through the same PYTHIA8-DELPHES chain as the signal events.

4 Detector simulation

The IDEA detector concept is a proposal for a general-purpose detector for the FCC-ee. The design includes an inner detector composed of 5 Monolithic silicon pixel (MAPS) layers followed by a high-transparency and high-resolution drift chamber. Outside the inner detector is located a high-resolution dual readout crystal calorimeter, surrounded by a superconducting solenoid producing a 2 T magnetic field. Outside the solenoid is a high granularity fiber dual-readout hadronic calorimeter, followed by three μ -rwall layers for muon detection, embedded in the return yoke of the solenoid.

The present study relies on the parameterised simulation in DELPHES of the inner detector for the estimate of the tracking and vertexing performance of IDEA, and on a simple energy response parametrisation for the electromagnetic calorimeter.

The vertex detector is simulated as 5 cylindrical layers with radius between 1.2 and 31.5 cm with 2-D readout, and resolution $3\text{ }\mu\text{m}$ except the outermost layer with a resolution of $7\text{ }\mu\text{m}$, and 3 disks in each of the forward/backward regions with a resolution of $7\text{ }\mu\text{m}$. The drift chamber is modelled as 112 co-axial layers, arranged in 24 identical azimuthal sectors, at alternating-sign stereo angles ranging from 50 to 250 mrad, and an assumed resolution on the single measurement of $100\text{ }\mu\text{m}$. The chamber has a length of 4 meters, and covers the radius between 34 cm and 2 m, yielding full tracking efficiency for polar angles θ larger than about 10 degrees. The DELPHES simulation software relies on a full description of this geometry and accounts for the finite detector resolution and for the multiple scattering in each tracker layer. Based on the measured ‘hits’ in the different layers, it turns charged particles emitted within the angular acceptance of the tracker into five-parameter tracks (the helix parameters that describe the trajectory of the particle, including the transverse and longitudinal impact parameters), and determines the full covariance matrix of these parameters. Details on the procedure are provided in [16]. Vertices are reconstructed using these tracks as input, based on a simple χ^2 minimisation with constraints, yielding 3D vertexes with their χ^2 (χ^2_{vx}/ndf) and covariance matrix. More details on the vertexing code used here can be found in [17].

For the crystal electromagnetic calorimeter a gaussian smearing is applied to deposited electromagnetic energy with the resolution parametrised as [18] (E in GeV):

$$\frac{\sigma(E)}{E} = \frac{0.03}{\sqrt{E}} \oplus 0.005 \oplus \frac{0.002}{E}. \quad (4.2)$$

5 Analysis

The final state for the signal addressed in the present analysis

$$e^+e^- \rightarrow \gamma A', A' \rightarrow \mu^+\mu^-$$

includes two opposite charge muons and a photon. The invariant mass of the two muons $m_{\mu^+\mu^-}$ has a narrow peak at the mass of the A' , with the width of the peak dominated by the experimental resolution on the reconstruction of $m_{\mu^+\mu^-}$.

The photon recoiling against a dark photon of mass $m_{A'}$ has a fixed energy E_{rec} , determined by the recoil formula:

$$E_{rec} = \frac{E_{CM}^2 - m_{A'}^2}{2 E_{CM}}, \quad (5.3)$$

where E_{CM} is the center-of-mass-energy in of the collisions.

The starting requirement in the analysis is the presence of exactly two reconstructed muons with energy above 2 GeV and of a photon with energy in excess of 5 GeV within the angular acceptance of the tracking detector.

In order to suppress reducible backgrounds, a preselection is applied requiring that the invariant mass of the two muons and the photon be larger than 90 GeV, and that the two muon tracks form a good vertex ($\chi_{vx}^2/ndf < 10$) inside the geometrical acceptance of the IDEA inner detector.

Two different analyses are developed from this point, with different strategies for the separation of signal and background, a prompt search, and a long-lived search.

The prompt search applies no requirement on the distance of the reconstructed $\mu^+\mu^-$ vertex from the interaction point d_{vx} , and relies on a detailed analysis of the final state kinematics to suppress the large $e^+e^- \rightarrow \gamma\mu^+\mu^-$ SM background. This analysis covers the complete mass range from 0.4 GeV to 360 GeV.

The long-lived search addresses the case where the A' decays after an observable path in the detector. A selection on d_{vx} can in principle fully eliminate the dominating SM prompt background, leaving only decays from heavy flavours which have a very different final state kinematics from the signal. As shown in Figure 3, this branch of the analysis only covers a limited mass range, but may probe lower values of the couplings than the prompt analysis.

In the following sections the two analyses will be described in detail.

5.1 Prompt analysis

For the prompt analysis, after the preselection is applied, the background is expected to be dominated by the SM process $e^+e^- \rightarrow \gamma\mu^+\mu^-$ which is abundantly produced, and has the same final state as the signal.

The initial step in the selection is the requirement, for each dark photon test mass $m_{A'}$ considered, that the event kinematics is compatible with a photon recoiling against a massive particle with mass $m_{A'}$.

To this effect, for each event the variable M_{cut} can be built as:

$$M_{cut}^2 = \frac{(m_{\mu^+\mu^-} - m_{A'})^2}{\sigma(m_{\mu^+\mu^-})^2} + \frac{(E_\gamma - E_{rec})^2}{\sigma(E_\gamma)^2}, \quad (5.4)$$

where E_{rec} is defined in Equation 5.3, and $\sigma(m_{\mu^+\mu^-})$ and $\sigma(E_\gamma)$ are respectively the expected muon-muon mass resolution, and photon energy resolution. The dependence

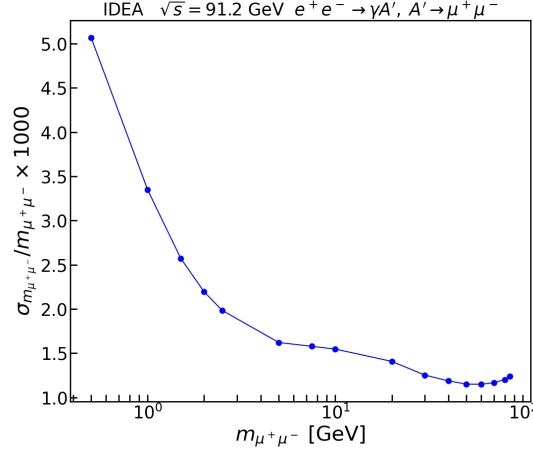


Fig. 4 Relative mass resolution for muon pairs from the of A' multiplied by 1000 as a function of $m_{\mu^+\mu^-}$.

of $\sigma(E_\gamma)$ on $m_{\mu^+\mu^-}$ can be calculated as the convolution of Eq. 4.2 and Eq. 5.3. It is approximately flat at 0.7% up to $m_{\mu^+\mu^-} \sim 40$ GeV and shoots up to a few percent as $m_{\mu^+\mu^-}$ approaches m_Z . The value of $\sigma(m_{A'})$ depends on the kinematics of the events. Its dependence on $m_{\mu^+\mu^-}$ is shown in Figure 4. The resolution varies smoothly between 0.1 and 0.15% above 5 GeV, and increases up to 0.5% at 0.5 GeV, when the uncertainty on the distance between the two muon tracks becomes the dominant factor in the mass measurement.

The discriminant variable M_{cut} is approximately independent of $m_{A'}$, and has an excellent signal to background separation power. The distributions of M_{cut} , truncated at a value of 10, and of $\log_{10}(M_{cut})$ are shown for $m_{A'} = 40$ GeV in Figure 5, for both signal and background at $\sqrt{s} = 91.2$ GeV. The selection $M_{cut} > 2$ approximately optimises the signal/background separation at all masses.

Given the relative values of the two components, and their dependences on $m_{\mu^+\mu^-}$, the rejection power of M_{cut} will be dominated by $\sigma(m_{\mu^+\mu^-})$ except for the very lowest values of $m_{A'}$. The sensitivity of the analysis is therefore mainly determined by the performance of the tracking system.

Besides the selection on M_{cut} , additional separation power between signal and background can be obtained through a detailed study of the angular distributions of the final state particles.

Each event is fully defined by 9 variables, i.e. the three-momenta of the two muons and the photon. The energy and momentum constraints from the e^+e^- collision reduce the independent variables to five. The signal is a photon accompanying a particle undergoing a two-body decay, and a convenient choice of variables is the invariant mass of the $\mu^+\mu^-$ pair, the angular coordinates θ_γ and ϕ_γ of the photon from the $e^+e^- \rightarrow \gamma A'$ production in the lab frame, and θ_{μ_1} and ϕ_{μ_1} , the coordinates of the leading muon, calculated in the rest frame of the $\mu^+\mu^-$ pair. Given the cylindrical symmetry of the system around the beam axis, the events can be rotated in such a

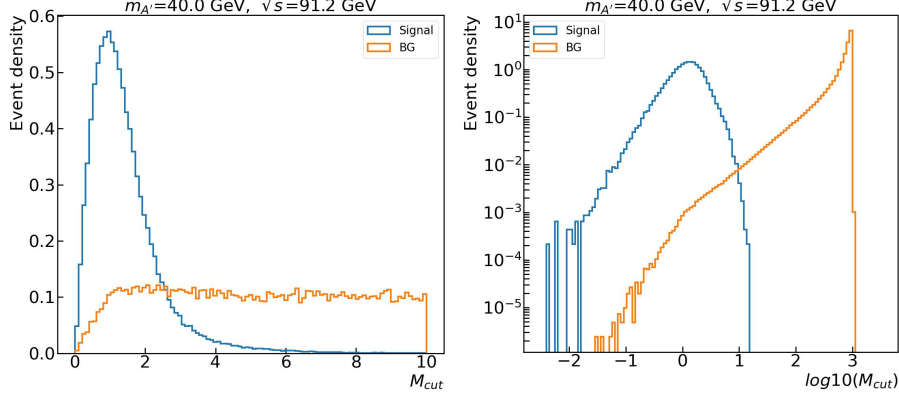


Fig. 5 Distribution of the variables M_{cut} truncated at 10 (left) and $\log_{10}(M_{cut})$ for signal (blue) and background (orange) for $m_{A'} = 40$ GeV.

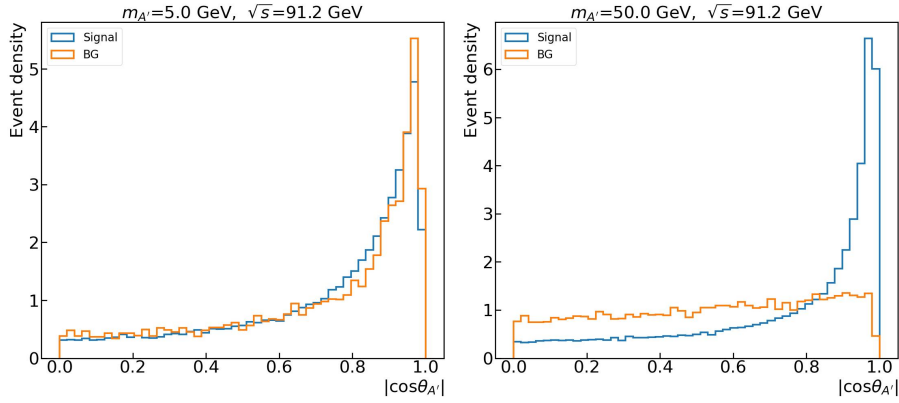


Fig. 6 Distribution of the variable $|\cos \theta_{A'}|$ for signal (blue) and background (orange) for two values of $m_{A'}$, 5 (left) and 50 (right) GeV.

way that $\phi_\gamma = 0$. After this rotation, the event is fully defined by $m_{\mu^+\mu^-}$ and by three angular variables. A reasonable choice is $\cos \theta_\gamma = -\cos \theta_{A'}$, $\cos \theta_{\mu_1}$ and ϕ_{μ_1} . The latter two are calculated in the A' rest frame. After inspecting the variables, $\cos \theta_{\mu_1}$ was replaced by two variables in the laboratory frame that encode equivalent information on the A' decay kinematics: the ratio of the energies of the two muons, E_{μ_2}/E_{μ_1} , and the cosine of their angular distance in 3-d space, $\cos \Delta\alpha_{\mu_1\mu_2}$, which provide better background discrimination. The distributions of the four discriminant variables defined above are shown in Figures 6-9 for two different test masses and for both signal and background for $\sqrt{s} = 91.2$ GeV. The selection $M_{cut} < 2$ has been applied for both signal and background.

The discrimination power is higher for $m_{A'} = 50$ GeV than for $m_{A'} = 5$ GeV. The difference is due to the fact that for masses much lower than m_Z the $\mu^+\mu^-$ pair results from the decay of a particle with photon-like couplings [5], and the background is dominated by a virtual photon going into $\mu^+\mu^-$. When $m_{A'}$ becomes comparable to

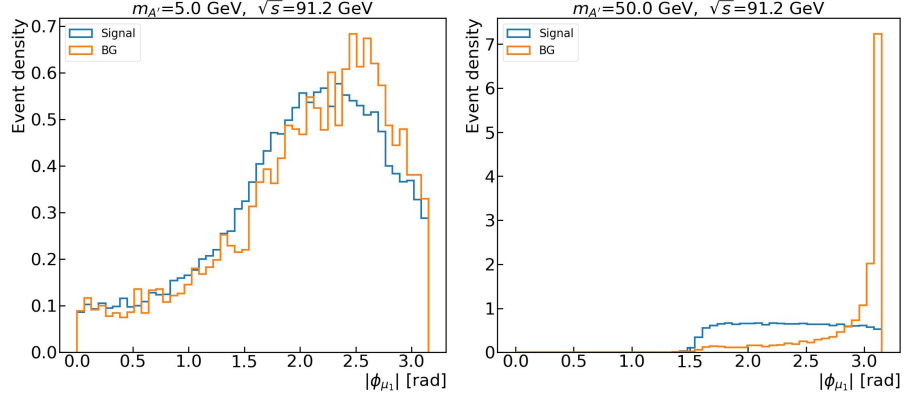


Fig. 7 Distribution of the variable $|\phi_{\mu_1}|$ calculated in the rest frame of the ALP for signal (blue) and background (orange) for two values of $m_{A'}$, 5 (left) and 50 (right) GeV.

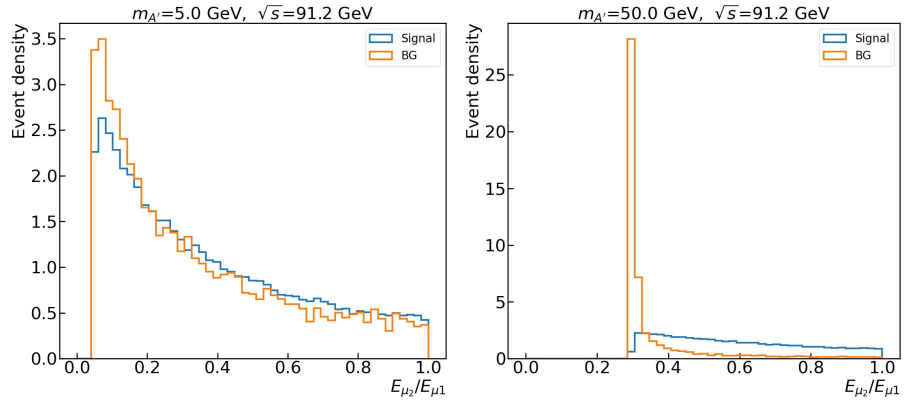


Fig. 8 Distribution of the variable E_{μ_2}/E_{μ_1} calculated for signal (blue) and background (orange) for two values of $m_{A'}$, 5 (left) and 50 (right) GeV.

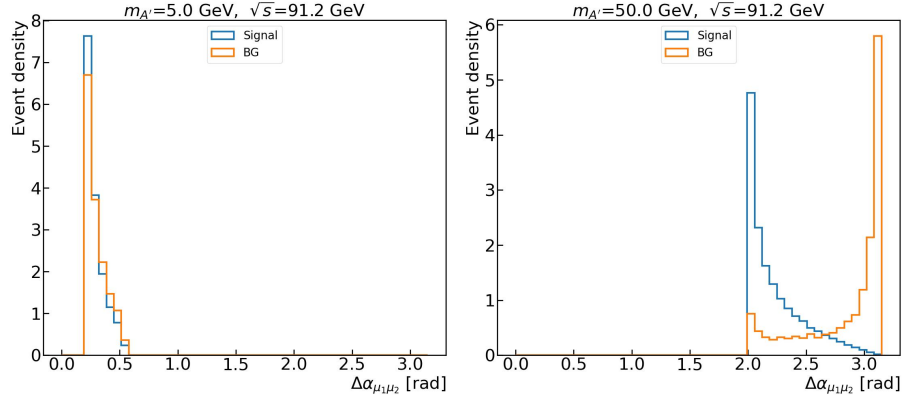


Fig. 9 Distribution of the variable $\cos \Delta\alpha_{\mu_1\mu_2}$ calculated for signal (blue) and background (orange) for two values of $m_{A'}$, 5 (left) and 50 (right) GeV.

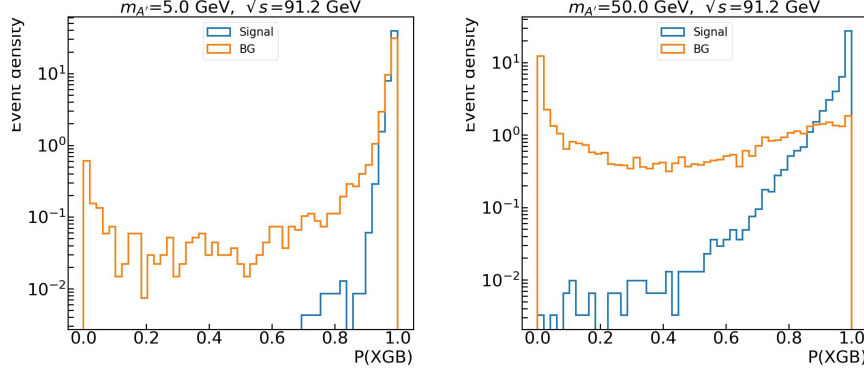


Fig. 10 Distribution of the variable P_{XGB} for signal (blue) and background (orange) for $m_{A'} = 5$ (left) and 50 (right) GeV.

m_Z , there is an admixture of photon and Z contributions with a relative ratio which evolves in a different way for signal and background, generating a difference in the angular distributions. For similar reasons, for values of \sqrt{s} different from the Z -pole, the analysis based on angular variables is in general less powerful than in the case of the Z -pole run.

For each test mass a signal selection is developed, starting from the preselection described above, based on the following steps:

- A boosted decision tree (XGBoost [19], XGB in the following) is trained on four variables, $|\cos \Delta\alpha_{\mu_1\mu_2}|$, E_{μ_2}/E_{μ_1} , $|\cos \theta_{A'}|$, and $|\phi_{\mu_1}|$, where the last variable is in the rest frame of the (μ_1, μ_2) system. The distributions of the discriminant variables depend on $m_{A'}$. Therefore, for each test value of $m_{A'}$, the samples of signal and background events used for training are requested to satisfy the condition $|m_{\mu_1\mu_2} - m_{A'}| < 5$ GeV ($M_{cut} < 10$) for $m_{A'} > (\leq) 10$ GeV respectively. The selections are aimed at ensuring a final state kinematics as close as possible to the one for the target signal, while retaining enough Monte Carlo events in the training and test samples as to ensure a statistically stable selection.
- The XGB probability (P_{XGB}) is then calculated on signal and background test samples for each target $m_{A'}$. An example distribution of the XGB probability (P_{XGB}) for $m_{A'} = 5$ and 50 GeV is shown in Figure 10 for events with $M_{cut} > 2$.
- For each FCC-ee run, the number of events in the test sample is normalised to the expected running statistics. For $m_{A'} < 10$ GeV the value of $BR(A' \rightarrow \mu^+\mu^-)$ calculated in [5] is used. The statistical significance Z_{stat} , defined as in [20] is calculated as a function of P_{XGB} for events passing the mass selection $M_{cut} < 2$.
- For each A' test mass and each centre-of-mass energy of the FCC-ee, the cut on P_{XGB} yielding the optimal sensitivity is determined, and the value of the coupling ϵ yielding a statistical significance $Z_{stat} = 2$ is calculated.

After the XGB selection, the total efficiency for the signal is $\sim 30 - 40\%$ over the full considered mass range, whereas the efficiency for the background has a strong dependence on $m_{A'}$. The number of expected signal and background events for the

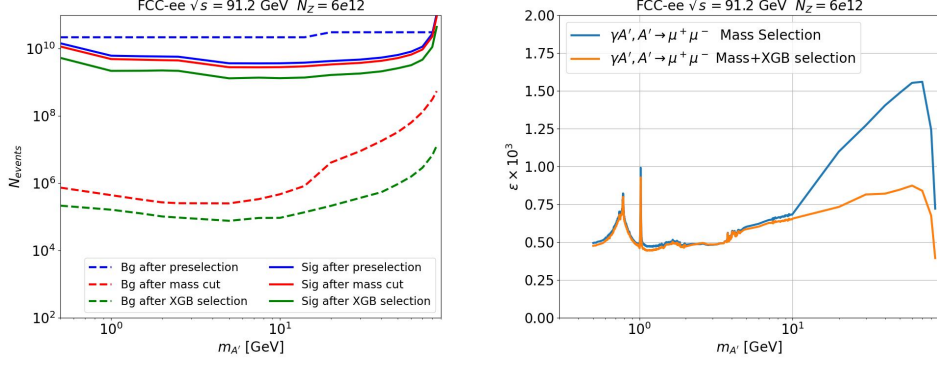


Fig. 11 Left: number of expected signal (full line) and background (dashed line) events for the FCC-ee Z-pole run and each of the selection steps described in the text. The lines after the XGB selection are given for a selection on P_{XGB} yielding an efficiency for the signal of 50% with respect to the mass selection. Right: experimental 95% reach on the mixing parameter ϵ as a function of $m_{A'}$. The blue line gives the result after the mass cut, and the orange line after the XGB cut.

FCC-ee Z-pole run after each of the selection steps described above is shown in the left side of Figure 11. The assumed value of the mixing for the signal is $\epsilon = 1$. The lines after the XGB selection are given for a selection on P_{XGB} yielding an efficiency for the signal of 50% with respect to the previous selection, approximately corresponding to the optimal selection for $m_{A'} > 20$ GeV. A strong dependence of the efficiency of the mass cut on $m_{A'}$ is observed for the background. For $m_{A'} \leq 10$ GeV the background rejection power of the XGB selection decreases with decreasing $m_{A'}$, and it does not improve the experimental reach below $m_{A'} \simeq 5$ GeV. The experimental 95% CL reach on the mixing parameter ϵ as a function of $m_{A'}$ is shown on the right side of Figure 11 for the FCC-ee Z-pole run. The result is shown for the mass selection alone and for the mass selection supplemented by the XGB selection, where the cut on P_{XGB} is set for each test value of $m_{A'}$ at the value optimising the sensitivity. A 95% CL sensitivity limit on ϵ varying between 0.5×10^{-3} and 0.85×10^{-3} is achieved throughout the mass range.

5.2 Long-lived analysis

In Section 2 it was shown that there is a region in the $m_{A'} - \epsilon$ parameter space where a detectable number of long-lived dark photons may be produced at the Z-pole run of the FCC-ee. For the present analysis, it is required that the A' decays inside the inner the tracker of the IDEA experiment. A quantitative idea of the accessible area in parameter space can thus be obtained by calculating for each point of the $m_{A'} - \epsilon$ space the integral of the expected number of events with a path in the detector d_{vx} in the range 0.5-2000 mm for the expected statistics of the FCC-ee Z-pole run. The results are shown in Figure 12, where the area for which at least three events are produced is bounded with a red line. The accessible mass range extends up to approximately 1.5 GeV, over a range of ϵ between a few 10^{-5} and a few 10^{-4} , dependent on $m_{A'}$, beyond the sensitivity of the prompt analysis. As explained in Section 2, when $m_{A'}$ is

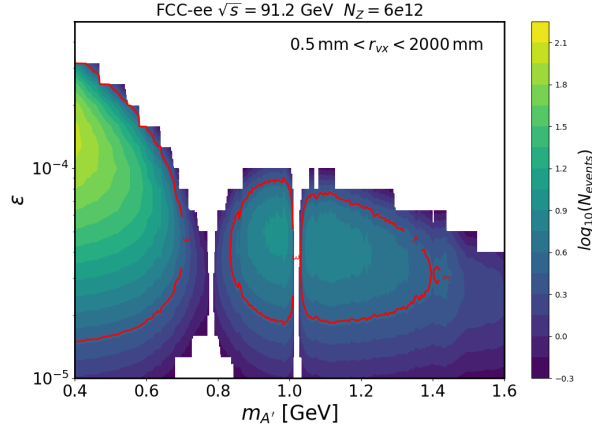


Fig. 12 Number of events decaying in the tracker of IDEA at a minimum distance of 0.5 mm from the center of the detector for the Z -pole run of FCC-ee in the $m_{A'} - \epsilon$ plane. The contour for three events is shown as a red line.

near the masses of the ω and ϕ resonances, the A' decays dominantly into hadrons, and it has a shorter lifetime. As a result the number of long-lived $A' \rightarrow \mu^+\mu^-$ decays is suppressed, generating the discontinuities in the area of expected sensitivity which can be seen in Figure 12.

The next step in the analysis is a Monte Carlo study to verify whether the produced long-lived dark photons can be separated from the SM background using the proposed IDEA detector.

The events are first requested to pass the same initial preselection as for the prompt analysis.

Reducible backgrounds from $e^+e^- \rightarrow \gamma\tau^+\tau^-$ with each τ decaying into $\mu\nu\bar{\nu}$ and $e^+e^- \rightarrow \gamma b\bar{b}$, could give rise to final state signatures with a photon and a $\mu^+\mu^-$ pair detached from the interaction vertex. No event from the generated Monte Carlo samples for these processes passes the kinematic preselections and has an invariant mass in the interval 0.4-1.6 GeV, except a single $\tau^+\tau^-$ event, which is removed by the vertex cleaning cuts described below. No explicit simulation was performed for $e^+e^- \rightarrow \gamma c\bar{c}$ which is expected to be smaller than $e^+e^- \rightarrow \gamma b\bar{b}$. These backgrounds are considered negligible for the following discussion.

The irreducible prompt background $e^+e^- \rightarrow \gamma\mu^+\mu^-$ can be suppressed by applying a lower cut the transverse distance of the reconstructed vertex r_{vx} from the centre of the detector. The variable in the plane transverse to the beam is used rather than the three dimensional variable d_{vx} , because the position of the interaction vertex, for the present design of the FCC-ee collider [21], has a spread of ~ 0.4 mm in the z coordinate, as opposed to the x and y coordinates which have spreads below a few microns.

A lower limit on r_{vx} should reduce to zero the number of prompt background events. The key performance figure is in this case the quality of the reconstruction

of r_{vx} in the IDEA tracker for a vertex with two collimated high momentum muon tracks, which determines how low the threshold on r_{vx} can be.

The distributions of r_{vx} in the mass windows of $m_{\mu^+\mu^-}$ around 0.6 and 1.1 GeV are shown in Figure 13 for signal and prompt background. The values of $m_{A'}$ and ϵ for the signal are chosen to match the points with maximum number of signal events in Figure 12.

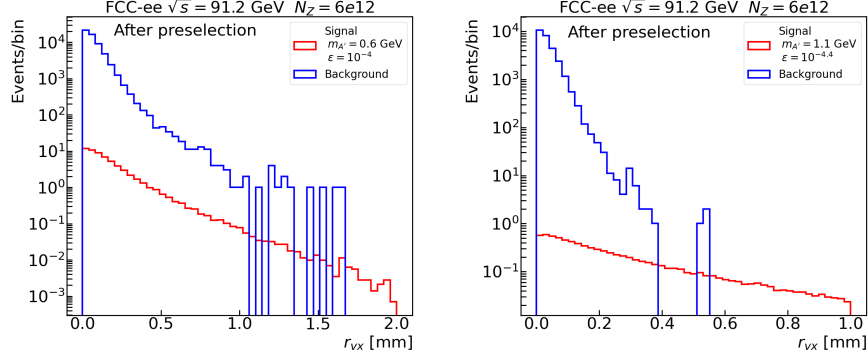


Fig. 13 Distribution of r_{vx} for signal and background for two values of $m_{A'}$, 0.6 (left) and 1.1 GeV (right) after the preselection cuts. The events are selected in $m_{\mu^+\mu^-}$ windows in of 10 MeV around the the nominal $m_{A'}$, and are normalised to the expected FCC-ee Z -pole run statistics.

Large non-gaussian tails towards high values of r_{vx} are observed for the background, whereas the distribution for the signal is determined by the expected flight path of the A' . The effect is particularly clear for $m_{\mu^+\mu^-}$ 0.6 GeV. In this situation, the cut on r_{vx} necessary to suppress the background level to a few events would also reduce the number of signal event below the detectable level.

The tails in the background r_{vx} are from events where the detector fails to reconstruct correctly the position of the vertex formed by the tracks of the muon pair in the event.

It is thus necessary to reject events which have a high probability that r_{vx} is badly measured. Useful variables to perform this selection were found to be the energy of the softer muon E_{μ_2} and the maximum pseudorapidity of the two muons $\max(|\eta_{\mu_1}|, |\eta_{\mu_2}|)$. Events where r_{vx} is badly measured have a low value of E_{μ_2} and a high value of $\max(|\eta_{\mu_1}|, |\eta_{\mu_2}|)$. This is shown in Figure 14, where the two variables are plotted for the prompt background in the mass range of interest of the LLP analysis $0.4 < m_{\mu^+\mu^-} < 2$ GeV. For this background the truth value of r_{vx}^{true} is determined by the beam transverse spread and is smaller than $2.5 \mu\text{m}$, therefore events with $r_{vx} > 0.2$ mm are badly measured. The selections $\max(|\eta_{\mu_1}|, |\eta_{\mu_2}|) < 2$ and $E_{\mu_2} > 6$ GeV strongly reduce background events with $r_{vx} > 0.2$ mm.

Another useful variable is $\Delta\phi_{vx A'}$, the angular distance in the transverse plane between the A' candidate and the vector connecting the centre of the detector and the position of the reconstructed vertex. In the case where the x and y coordinates of the real muon-muon vertex are equal to zero, the reconstructed vertex can be

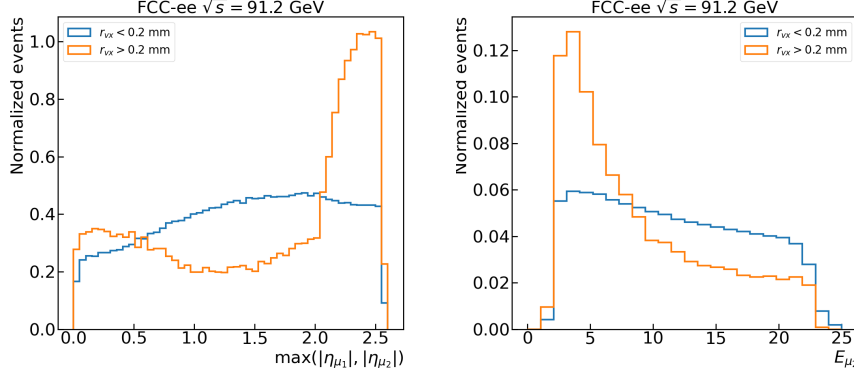


Fig. 14 Distribution of the variables: left: $\max(|\eta_{\mu_1}|, |\eta_{\mu_2}|)$, right: E_{μ_2} for $r_{vx} > 0.2$ mm (orange) and $r_{vx} < 0.2$ mm (blue) for the background $e^+e^- \rightarrow \gamma\mu^+\mu^-$ and $0.4 < m_{\mu^+\mu^-} < 2$ GeV.

either in the same hemisphere of the two reconstructed muons or in the opposite hemisphere, with approximately equal probability. In the case where the real two-muon vertex is detached from the beam direction, $\cos \Delta\phi_{vx A'}$ is predominantly positive. A requirement $\cos \Delta\phi_{vx A'} > 0.95$ reduces by a factor two the background with badly measured r_{vx} , and has approximately 100% efficiency on the signal. The combined requirements $\max(|\eta_{\mu_1}|, |\eta_{\mu_2}|)$, E_{μ_2} and $\cos \Delta\phi_{vx A'}$ will be collectively called ‘vertex cleaning cuts’ in the following.

The impact of the vertex cleaning cuts can be observed in Figure 15, where the r_{vx} distributions are plotted for the same signal and background samples as for Figure 13. The badly measured events generating high values of r_{vx} are effectively removed, with

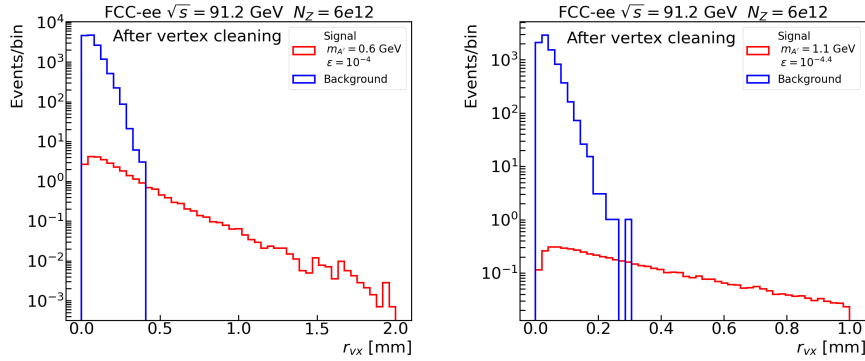


Fig. 15 Distribution of r_{vx} for signal and background for two values of $m_{A'}$, 0.6 (left) and 1.1 GeV (right) after the vertex cleaning cuts. The events are selected in $m_{\mu^+\mu^-}$ windows of 10 MeV around the nominal $m_{A'}$, and are normalised to the expected FCC-ee Z -pole run statistics.

a small reduction on the signal efficiency for high r_{vx} . For the final sensitivity, it is necessary to define as a function of $m_{\mu^+\mu^-}$ the optimal cut on r_{vx} , based on the

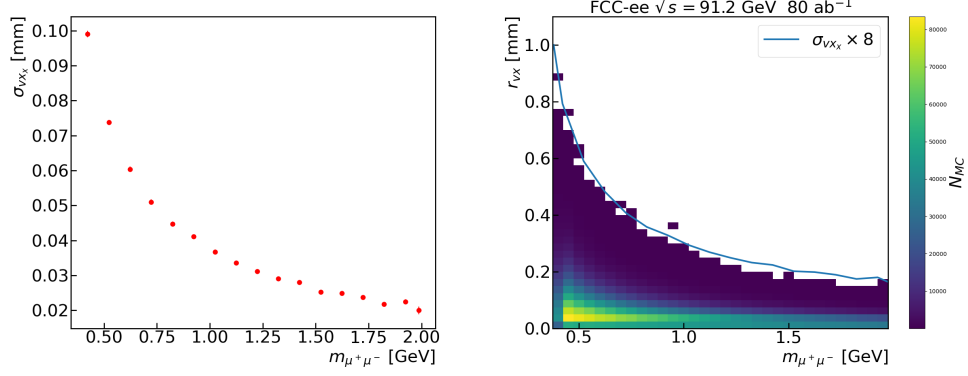


Fig. 16 Left: Resolution on the x component of the vertex position as a function of $m_{\mu^+\mu^-}$ after the vertex selections described in the text, for the background $e^+e^- \rightarrow \gamma\mu^+\mu^-$. Right: number of MC background events passing in the $m_{\mu^+\mu^-} - r_{vx}$ plane. Superimposed in blue is the curve corresponding to eight times the resolution on vx_x .

resolution on the r_{vx} measurement $\sigma_{r_{vx}}$. A detailed study on $\sigma_{r_{vx}}$ was performed using the parametrised simulation of the IDEA tracker.

The dependence of the resolution on the x component of the vertex position on $m_{\mu^+\mu^-}$ for the prompt background after the vertex cleaning cut is shown in the right panel of Figure 16. The resolution σ_{vx_x} is $\sim 100 \mu\text{m}$ for $m_{\mu^+\mu^-} = 0.4 \text{ GeV}$, and it becomes $\sim 20 \mu\text{m}$ for $m_{\mu^+\mu^-} = 2 \text{ GeV}$. If the number of MC background events passing the vertex selections is plotted in the $m_{\mu^+\mu^-} - r_{vx}$ plane, practically no events have r_{vx} exceeding the calculated σ_{vx_x} distribution multiplied by 8. This is shown in the left panel of Figure 16.

On this basis, the long-lived $A' \rightarrow \mu^+\mu^-$ candidates are selected by requiring $r_{vx} > 8 \times \sigma_{vx_x}(m_{\mu^+\mu^-})$.

Having thus defined a selection criteria for long-lived particles which minimises prompt background, the reach for the discovery of a long-lived A' can be evaluated. For each generated value of $m_{A'}$ and ϵ the signal efficiency is calculated by applying the vertex-related cuts and by requiring that $m_{\mu^+\mu^-}$ is in a window of $\pm 0.01 \text{ GeV}$ around $m_{A'}$. The resulting signal efficiency in the $m_{A'} - \epsilon$ plane is shown in Figure 17. The maximum efficiency is approximately 40%, with a strong dependence on the mixing parameter ϵ , which determines the fraction of the events decaying in the IDEA inner detector that satisfy the selection on r_{vx} .

The background estimate needs to compensate for the statistical fluctuations of the number of background events in the very narrow mass window, and for the fact that the available MC statistics is 40% of the expected statistics for the FCC-ee Z-pole run. A total of 5 MC background events in the mass range 0.4-1.6 GeV pass the long-lived selection. Assuming that they are equally distributed among each of the 0.02 GeV width mass bins, the estimated average number of background events per mass bin, scaled to the statistics of the FCC-ee Z run, is 0.21.

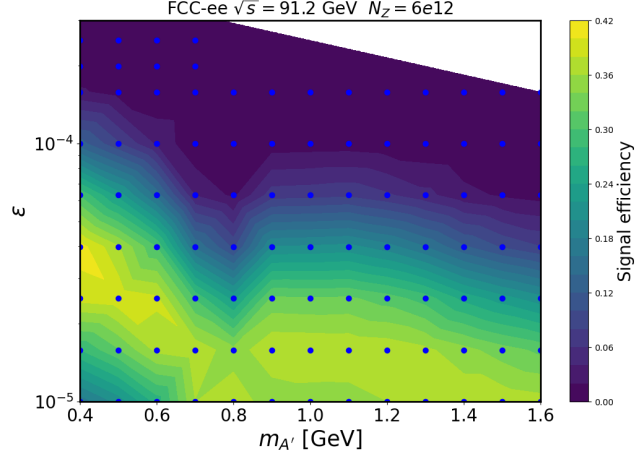


Fig. 17 Signal efficiency for the long-lived selection described in the text in the $m_{A'} - \epsilon$ plane.

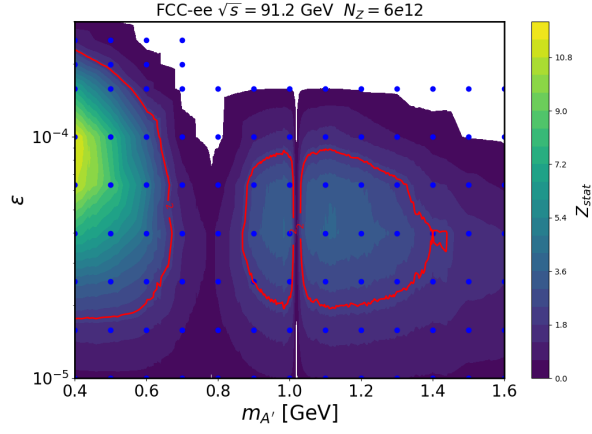


Fig. 18 Statistical significance Z_{stat} for the A' long-lived search in the $m_{A'} - \epsilon$ plane. The lines bounding the region where $Z_{stat} > 2$ are shown in red.

The final sensitivity (Z_{stat}) is calculated for each generated signal point from the estimated number of signal and background events normalised to the expected statistics of the FCC-ee Z -pole run, based on the prescriptions in [20]. The results are shown in Figure 18. The lines bounding the region where $Z_{stat} > 2$ are shown in red, corresponding to the 95% CL sensitivity for A' .

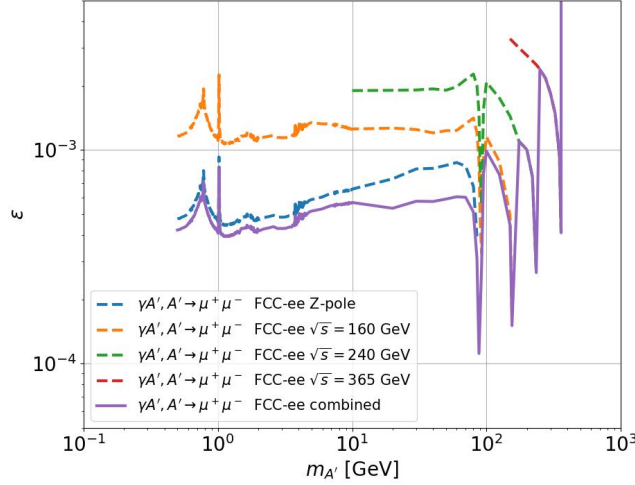


Fig. 19 Sensitivity limits at 95% confidence level in the $m_{A'} - \epsilon$ plane for the prompt analysis. The results for the different FCC-ee runs and for their statistical combination are shown.

6 Results and Conclusions

On the basis of the prompt analysis described in Section 5.1, the 95% confidence level sensitivity limits on the ϵ parameter were calculated for all of the four different \sqrt{s} runs of the FCC-ee. The results are shown in Figure 19.

The limits cover a mass range 0.5-360 GeV. The contributions of the different runs are statistically combined to yield the complete expected reach of FCC-ee running. In the mass region 10-85 GeV the Z-pole run yields the best sensitivity, as expected, but a significant improvement in reach is expected when combining the results with the data-taking at $\sqrt{s} = 160$ and 240 GeV.

The combined FCC-ee reach for both prompt and long-lived analysis is compared with the extrapolations for high-luminosity LHC (HL-LHC) for the CMS the LHCb experiments, and with the projected reach of the SHIP and Belle II experiments in Figure 20. For the CMS experiment, the extrapolation is calculated by scaling the expected reach in ϵ^2 for the published LHC Run 2 analyses [22, 23] by the square root of the ratio between 3 ab^{-1} , the design integrated luminosity for HL-LHC, and the integrated luminosity used for the analyses. For LHCb an extrapolation to HL-LHC is found in [24]. For SHIP and Belle II the projected reach is provided in [26] and [25] respectively.

In the mass interval 20-365 GeV, the expected FCC-ee sensitivity for the prompt analysis improves on the HL-LHC extrapolations.

The long-lived analysis covers the mass range between 0.4 and 1.4 GeV in interval of the mixing ϵ which is outside of the reach of the extrapolations of both the LHC and the beam-dump experiments. This is shown more clearly in Figure 21, where the relevant region in parameter space is shown with the mass in linear scale. This

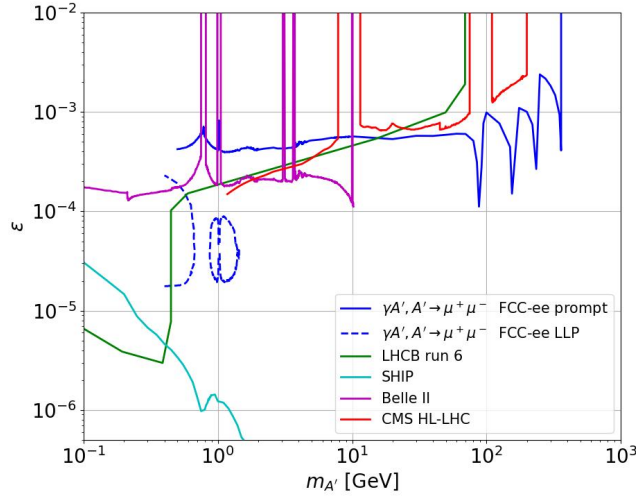


Fig. 20 Sensitivity limits at 95% confidence level in the $m_{A'} - \epsilon$ plane for the statistical combination of the FCC-ee runs compared to the HL-LHC extrapolations for CMS [22, 23] and LHCb [24] and to the projections for Belle II [25] and SHIP [26].

results crucially depends on the capability of the vertexing and tracking system of the experiment to measure with high precision the radial position of the vertex built out of two very collimated tracks, and it constitutes a severe benchmark for the design of a future detector at the FCC-ee.

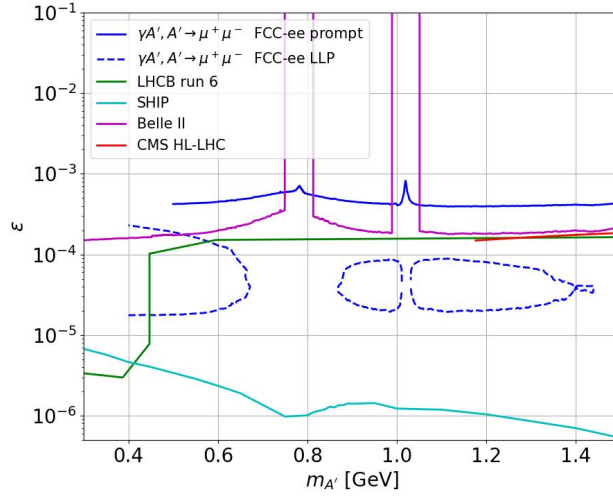


Fig. 21 Sensitivity limits at 95% confidence level in the $m_{A'} - \epsilon$ plane for the statistical combination of the FCC-ee runs compared to the HL-LHC extrapolations for CMS [22, 23] and LHCb [24] and to the projections for Belle II [25] and SHIP [26]. Zoom on the sensitivity region of the LLP analysis.

References

- [1] Abada, A., *et al.*: FCC-ee: The Lepton Collider: Future Circular Collider Conceptual Design Report Volume 2. Eur. Phys. J. ST **228**(2), 261–623 (2019) <https://doi.org/10.1140/epjst/e2019-900045-4>
- [2] Alexander, J., *et al.*: Dark Sectors 2016 Workshop: Community Report (2016) [arXiv:1608.08632](https://arxiv.org/abs/1608.08632) [hep-ph]
- [3] Battaglieri, M., *et al.*: US Cosmic Visions: New Ideas in Dark Matter 2017: Community Report (2017) [arXiv:1707.04591](https://arxiv.org/abs/1707.04591) [hep-ph]
- [4] Benedikt, M., *et al.*: Future Circular Collider Feasibility Study Report: Volume 1, Physics, Experiments, Detectors (2025) <https://doi.org/10.17181/CERN.9DKX.TDH9> [arXiv:2505.00272](https://arxiv.org/abs/2505.00272) [hep-ex]
- [5] Curtin, D., Essig, R., Gori, S., Shelton, J.: Illuminating Dark Photons with High-Energy Colliders. JHEP **02**, 157 (2015) [https://doi.org/10.1007/JHEP02\(2015\)157](https://doi.org/10.1007/JHEP02(2015)157) [arXiv:1412.0018](https://arxiv.org/abs/1412.0018) [hep-ph]
- [6] Fabbrichesi, M., Gabrielli, E., Lanfranchi, G.: The Dark Photon (2020) <https://doi.org/10.1007/978-3-030-62519-1> [arXiv:2005.01515](https://arxiv.org/abs/2005.01515) [hep-ph]
- [7] Graham, M., Hearty, C., Williams, M.: Searches for Dark Photons at Accelerators. Ann. Rev. Nucl. Part. Sci. **71**, 37–58 (2021) <https://doi.org/10.1146/>

- [8] He, M., He, X.-G., Huang, C.-K., Li, G.: Search for a heavy dark photon at future e^+e^- colliders. JHEP **03**, 139 (2018) [https://doi.org/10.1007/JHEP03\(2018\)139](https://doi.org/10.1007/JHEP03(2018)139) arXiv:1712.09095 [hep-ph]
- [9] Airen, S., Broadberry, E., Marques-Tavares, G., Ricci, L.: Vector portals at future lepton colliders. JHEP **08**, 029 (2025) [https://doi.org/10.1007/JHEP08\(2025\)029](https://doi.org/10.1007/JHEP08(2025)029) arXiv:2412.09681 [hep-ph]
- [10] Abbrescia, M., et al.: The IDEA detector concept for FCC-ee. arXiv:2502.21223 (2025) arXiv:2502.21223 [physics.ins-det]
- [11] Alwall, J., Frederix, R., Frixione, S., Hirschi, V., Maltoni, F., Mattelaer, O., Shao, H.-S., Stelzer, T., Torrielli, P., Zaro, M.: The automated computation of tree-level and next-to-leading order differential cross sections, and their matching to parton shower simulations. JHEP **07**, 079 (2014) [https://doi.org/10.1007/JHEP07\(2014\)079](https://doi.org/10.1007/JHEP07(2014)079) arXiv:1405.0301 [hep-ph]
- [12] <https://feynrules.irmp.ucl.ac.be/wiki/HAHM>
- [13] Sjöstrand, T., Ask, S., Christiansen, J.R., Corke, R., Desai, N., Ilten, P., Mrenna, S., Prestel, S., Rasmussen, C.O., Skands, P.Z.: An introduction to PYTHIA 8.2. Comput. Phys. Commun. **191**, 159–177 (2015) <https://doi.org/10.1016/j.cpc.2015.01.024> arXiv:1410.3012 [hep-ph]
- [14] Favereau, J., Delaere, C., Demin, P., Giammanco, A., Lemaître, V., Mertens, A., Selvaggi, M.: DELPHES 3, A modular framework for fast simulation of a generic collider experiment. JHEP **02**, 057 (2014) [https://doi.org/10.1007/JHEP02\(2014\)057](https://doi.org/10.1007/JHEP02(2014)057) arXiv:1307.6346 [hep-ex]
- [15] <https://github.com/HEP-FCC/FCC-config/tree/winter2023/FCCee>
- [16] Bedeschi, F., Gouskos, L., Selvaggi, M.: Jet flavour tagging for future colliders with fast simulation. Eur. Phys. J. C **82**(7), 646 (2022) <https://doi.org/10.1140/epjc/s10052-022-10609-1> arXiv:2202.03285 [hep-ex]
- [17] Bedeschi, F.: A vertex fitting package (2024) <https://doi.org/10.17181/hvcpv-bk752> arXiv:2409.19326 [hep-ex]
- [18] Lucchini, M.T., Pezzotti, L., Polesello, G., Tully, C.G.: Particle flow with a hybrid segmented crystal and fiber dual-readout calorimeter. JINST **17**(06), 06008 (2022) <https://doi.org/10.1088/1748-0221/17/06/P06008> arXiv:2202.01474 [hep-ex]
- [19] <https://xgboost.readthedocs.io/en/stable/>

- [20] ATLAS: Formulae for Estimating Significance. ATLAS Note ATL-PHYS-PUB-2020-025 available at <https://cds.cern.ch/record/2736148/files/ATL-PHYS-PUB-2020-025.pdf> (2020)
- [21] Benedikt, M., et al.: Future Circular Collider Feasibility Study Report: Volume 2, Accelerators, Technical Infrastructure and Safety (2025) <https://doi.org/10.17181/CERN.EBAY.7W4X> [arXiv:2505.00274](https://arxiv.org/abs/2505.00274) [physics.acc-ph]
- [22] Sirunyan, A.M., *et al.*: Search for a Narrow Resonance Lighter than 200 GeV Decaying to a Pair of Muons in Proton-Proton Collisions at $\sqrt{s} = \text{TeV}$. Phys. Rev. Lett. **124**(13), 131802 (2020) <https://doi.org/10.1103/PhysRevLett.124.131802> [arXiv:1912.04776](https://arxiv.org/abs/1912.04776) [hep-ex]
- [23] Hayrapetyan, A., *et al.*: Search for direct production of GeV-scale resonances decaying to a pair of muons in proton-proton collisions at $\sqrt{s} = 13 \text{ TeV}$. JHEP **12**, 070 (2023) [https://doi.org/10.1007/JHEP12\(2023\)070](https://doi.org/10.1007/JHEP12(2023)070) [arXiv:2309.16003](https://arxiv.org/abs/2309.16003) [hep-ex]
- [24] Craik, D., Ilten, P., Johnson, D., Williams, M.: LHCb future dark-sector sensitivity projections for Snowmass 2021 (2022) [arXiv:2203.07048](https://arxiv.org/abs/2203.07048) [hep-ph]
- [25] Kou, E., et al.: The Belle II Physics Book (2018) [arXiv:1808.10567](https://arxiv.org/abs/1808.10567) [hep-ex]
- [26] Ahdida, C., *et al.*: Sensitivity of the SHiP experiment to dark photons decaying to a pair of charged particles. Eur. Phys. J. C **81**(5), 451 (2021) <https://doi.org/10.1140/epjc/s10052-021-09224-3> [arXiv:2011.05115](https://arxiv.org/abs/2011.05115) [hep-ex]